Supplementary Information

Enhanced high-temperature electrochemical properties of in-situ carbon-coated truncated octahedral $LiMn_2O_4$ cathode

Jiayi He [a, b, ‡], Yan Ren [a, ‡], Shuxin Zhuang [a, *], Shengyu Jiang [a], Xiaoxiao Pan [a], Gaoxing Sun [a], Bin Zhu [a], Yanfen Wen [a, *], Xiaodan Li [a]

Theoretical calculations and experimental components

DFT theoretical calculation

Density functional theory (DFT) calculations based on First-Principles were used by Vienna Ab-initio Simulation Package (VASP) to optimize all atoms in the adsorption models to stable configurations [1-2]. The plane-wave energy cutoff was set to 500 eV and the energy was converged to 1.0×10^{-5} eV. Firstly, a 4 × 4 × 3 k-point grid of the $LiMn_2O_4$ adsorption model including 8 Li atoms, 32 O atoms and 16 Mn atoms was established, and a 10 Å vacuum layer was set up to avoid possible interactions between adjacent layers. And then the Monkhorst-Pack k-point grids were sampled to 2 × 2 × 2 in the computations of structure optimization and electronic properties.

Adsorption energy (ΔE_{ad}) is the energy released by C_2H_2 or N_2 molecules adsorbed

[a] *Key Laboratory of Functional Materials and Applications of Fujian Province, School of Materials Science and Engineering, Xiamen University of Technology, Xiamen 361024, China. E-mail: zsxtony@xmut.edu.cn (S. Zhuang), 2021000050@xmut.edu.cn (Y. Wen)*

[b] *Shanghai Xuanyi New Energy Development Co., Ltd., Shanghai 201806, China*

‡ *These authors contributed equally to this work.*

from the gas phase to $LiMn_2O_4$ surface, and ΔE_{ad} can be calculated from $\mathbf{\Delta E_{ad} = E_{Substrate/gas} - E_{Substrate} - E_{gas}}$ [3], where $E_{Substrate/gas}$, $E_{Substrate}$, and E_{gas} represent the total energy of substrate and adsorbed gas system, the energy of single substrate, and the energy of adsorbed gas molecule in the system, respectively. The greater the negative value of ΔE_{ad}, the easier it is for gas molecules to adsorb on the surface of $LiMn_2O_4$.

Synthesis of truncated octahedral $LiMn_2O_4$

The truncated octahedral $LiMn_2O_4$ was prepared via a facile and low-cost carbon template sol-gel method. Lithium acetate ($C_2H_3O_2Li{\cdot}2H_2O$, Aladdin, AR 99.0%), manganese acetate ($Mn(C_2H_3O_2)_2{\cdot}4H_2O$, Aladdin, AR 99.0%) and citric acid ($C_6H_8O_7{\cdot}H_2O$, Aladdin, GR 99.8%) were dissolved in deionized water at a molar ratio of 1:2:1 and magnetically stirred for 30 min. Weighed carbon black (Cabot, Vulcan XC-72R) according to the mass ratio of 0.5:1 to the target product and added it to deionized water containing 50 wt.% ethanol, and then mixed the solution with the Li-Mn mixed solution and stirred it well. After adjusting pH to 8.5 by adding ammonia, the mixed solution was heated in a water bath at 80 °C until it was mushy. Subsequently, the mushy gel was dried in an oven at 230 °C for 2 h to generate xerogel precursors. Following, the precursors were ground and then sintered at 750 °C at a heating rate of 2 °C/min for 10 h in the muffle furnace. Finally, the resulting powders were milled to produce $LiMn_2O_4$.

Synthesis of carbon coated truncated octahedral $LiMn_2O_4$

The uniform amorphous carbon coating truncated octahedral spinel $LiMn_2O_4$ was synthesized by CVD method using acetylene as carbon source. The prepared truncated

octahedral $LiMn_2O_4$ was firstly placed in a porcelain boat, and then alcohol was added to the vessel until the powder material was completely submerged. Following, the vessel was placed in a tubular furnace, and the temperature of the furnace was raised to 500 °C in a nitrogen atmosphere at a heating rate of 5 °C/min. Subsequently, acetylene was introduced at a small flow rate of 10 mL/min for 5 min, 10 min and 15 min, and then the $LiMn_2O_4$/C nanocomposites were obtained by natural cooling under nitrogen atmosphere, which were denoted as LMO/C-1, LMO/C-2 and LMO/C-3, respectively.

Material characterization

X-ray diffraction (XRD, X' pert PRO, Panalytical, Netherlands, Cu Kα, 1.54056 Å) was employed to investigate the phase of the samples from 10° to 70° (scanning speed: 10 °/min). Raman spectra (Raman, Labramhr, HORIBA Jobin Yvon) were carried out from 50 to 3000 cm^{-1} to explore the degree of graphitization. Scanning electron microscope (SEM, EVO18, Zeiss) and field emission transmission electron microscope (FE-TEM, Talos, FEI) with energy dispersive spectroscopy (EDS, Super-X energy dispersive spectrum, FEI) were conducted to recognize the morphology, structure and chemical component of the samples.

Electrochemical measurements

To prepare the working electrode, 80 wt.% of the as-prepared $LiMn_2O_4$/C nanocomposites, 10 wt.% of acetylene black (as a conductive agent) and 10 wt.% of polyvinylidene difluoride (PVDF, as a binder) dissolved in N-methyl-2-pyrrolidone (NMP) to form homogeneous slurry, which was then evenly plastered on an aluminum

foil (as the current collector) and dried in a vacuum oven at 120 °C for 12 h. And then pressed it at a pressure of 2 MPa, and cut it into small discs with a diameter of 12 mm. A lithium metal electrode was used as both the anode and reference electrode with an electrolyte of 1 M $LiPF_6$ that dissolved in a mixture of ethylene carbonate (EC), dimethyl carbonate (DMC), and diethyl carbonate (DEC) at a volume ratio of 1:1:1. The polypropylene separator (Celgard 2400) was ϕ16 mm. The mass load of active material is typically in the range of 0.95 ~ 1.1 mg/cm^2. The CR2025 coin-type half cells were assembled in an argon-filled glove box (< 0.01 ppm of O_2 and H_2O). Galvanostatic charge and discharge (GCD) measurements at different C rates (1 C is defined as 148 mA/g for $LiMn_2O_4$) were carried out in the voltage range between 3.0 and 4.3 V (vs. Li/Li^+) by NEWARE-CT-4008Tn battery tester. Cyclic voltammetry (CV) at different scan rates in a potential range between 3.0 and 4.45 V (vs. Li/Li^+) and electrochemical impedance spectroscopy (EIS) in the frequency range from 100 kHz to 0.01 Hz with an AC perturbation voltage of 5 mV were carried out by using electrochemical workstation (AUTOLAB-PGSTAT302N).

Fig. S1

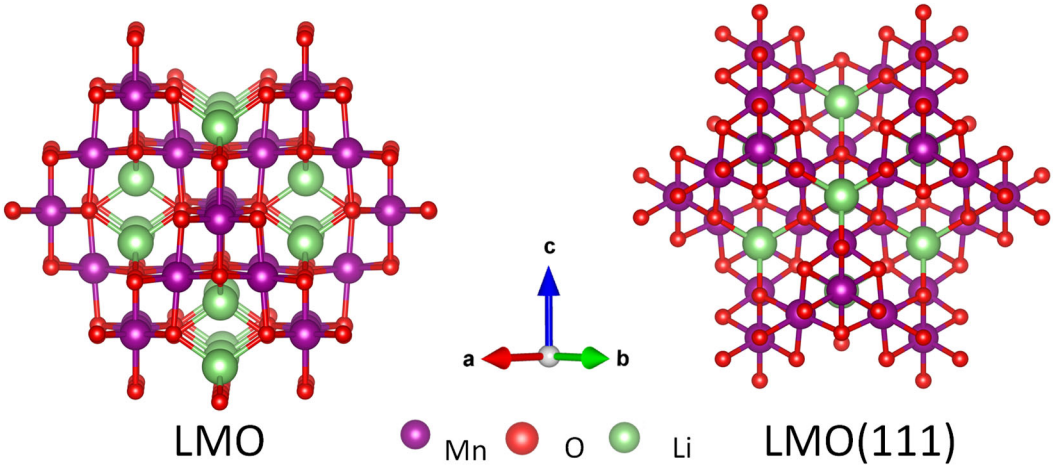

Fig. S1 The optimized structure model of $LiMn_2O_4$.

Fig. S2

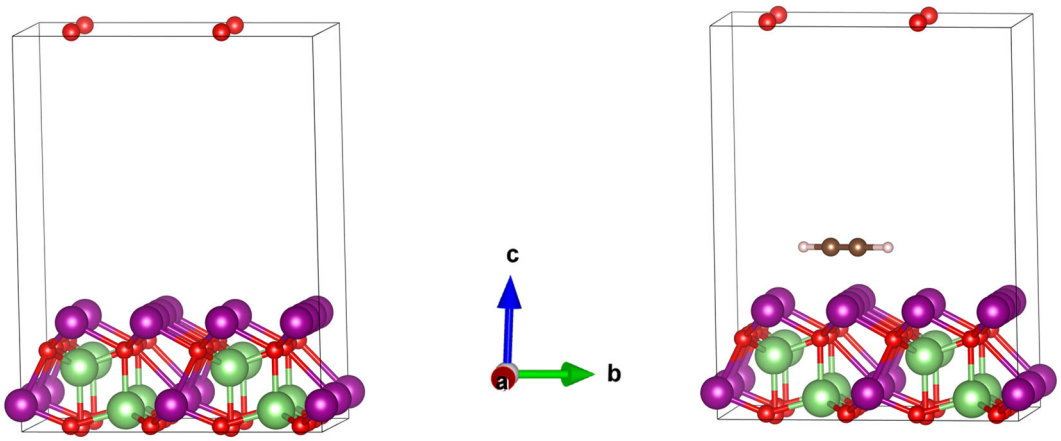

Fig. S2 The optimized structure model of $LiMn_2O_4/C_2H_2$ with a 10 Å vacuum layer.

Fig. S3

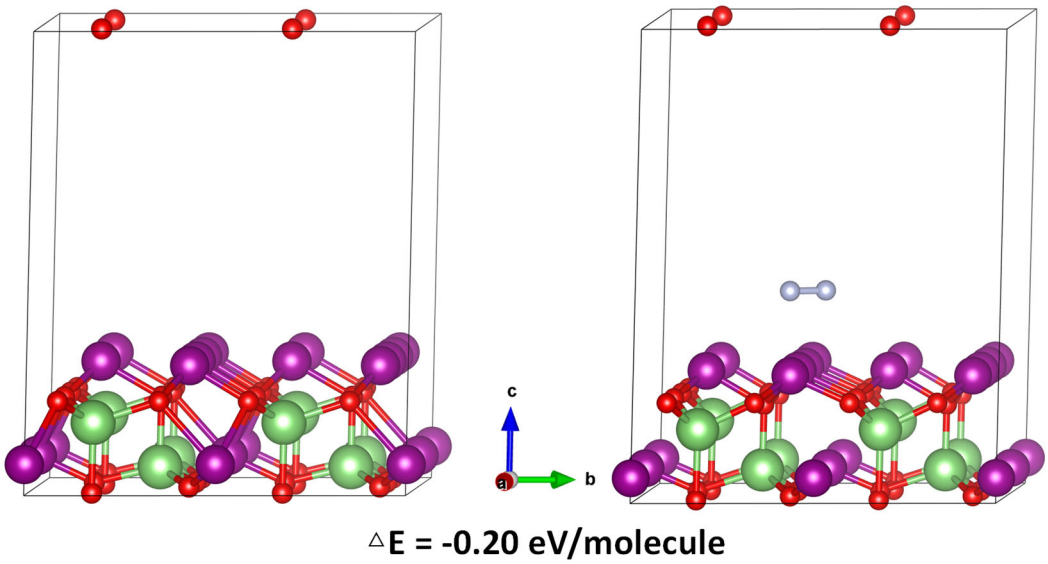

Fig. S3 The optimized structure model of $LiMn_2O_4/N_2$ with a 10 Å vacuum layer.

Fig. S4

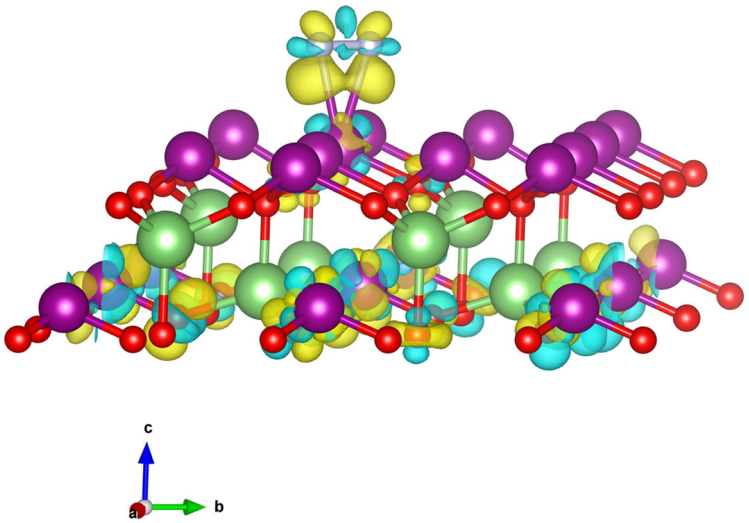

Fig. S4 DCD of $LiMn_2O_4/N_2$ system.

Fig. S5

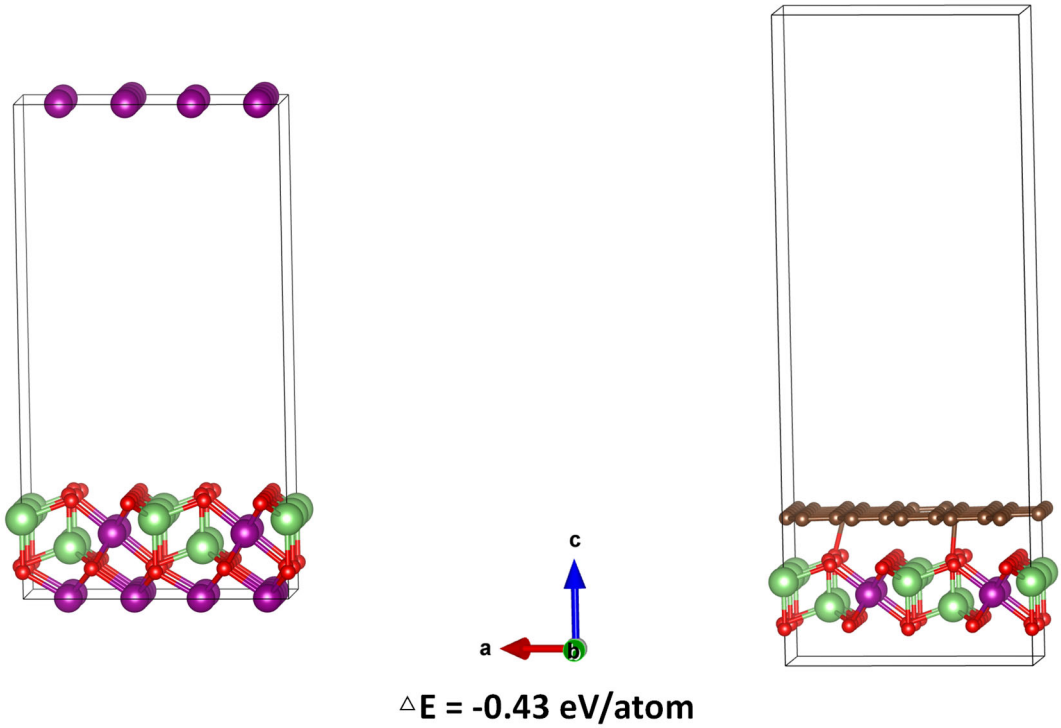

Fig. S5 The optimized structure model of $LiMn_2O_4$/C with a 15 Å vacuum layer.

Fig. S6

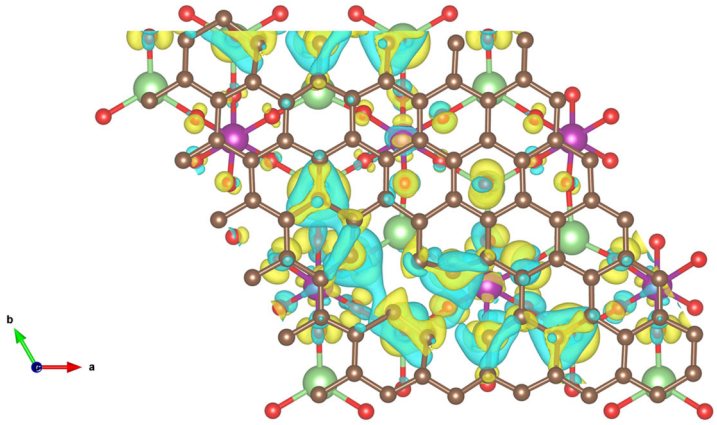

Fig. S6 The top view of DCD of $LiMn_2O_4$/C system.

Fig. S7

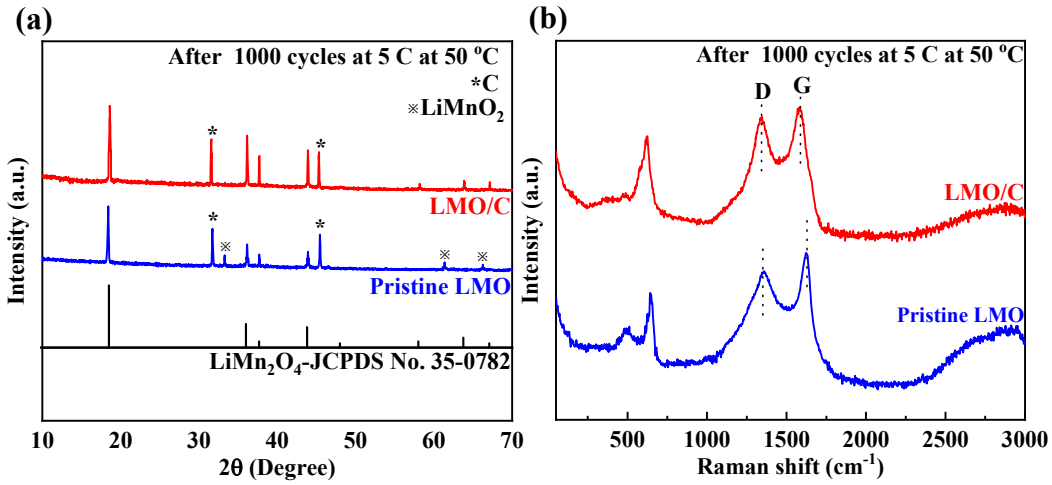

Fig. S7 XRD patterns (a), Raman spectra (b) of pristine LMO and LMO/C electrodes after 1000 cycles at 5 C at 50 °C.

Fig. S8

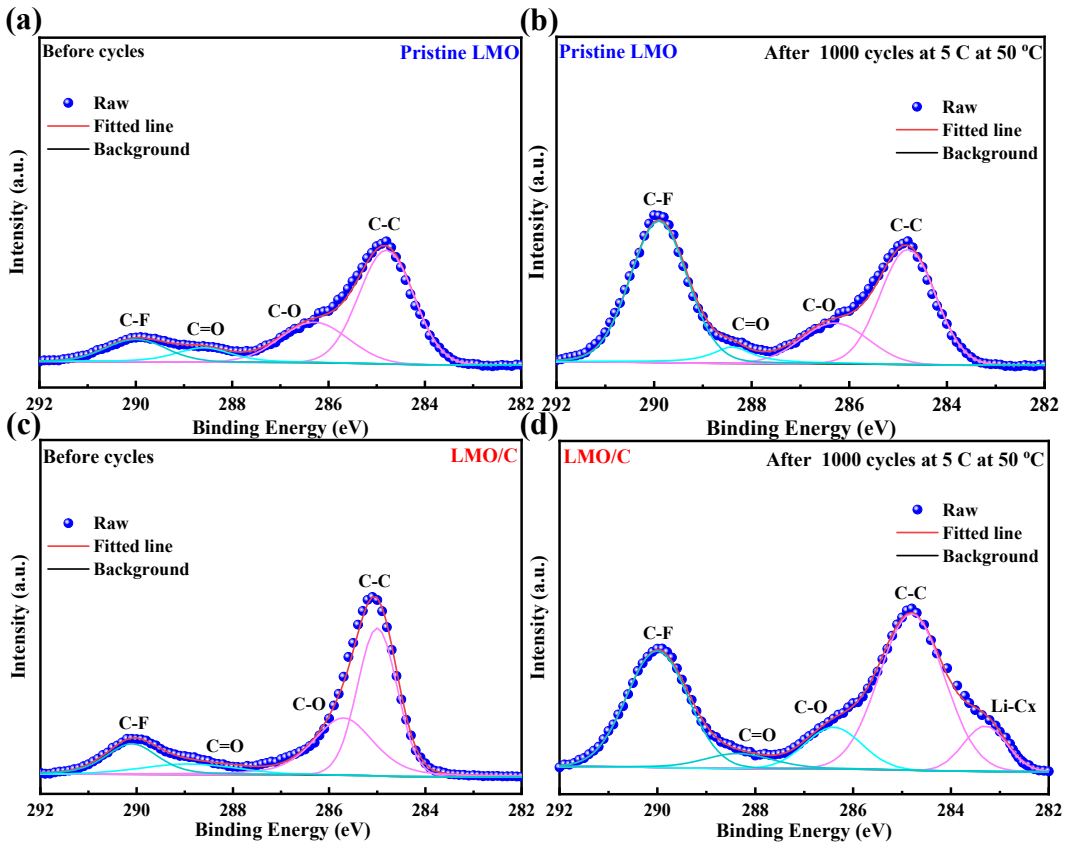

Fig. S8 The fitted profiles of C 1s peaks of pristine LMO and LMO/C electrodes before and after 1000 cycles at 5 C at 50 °C.

Fig. S9

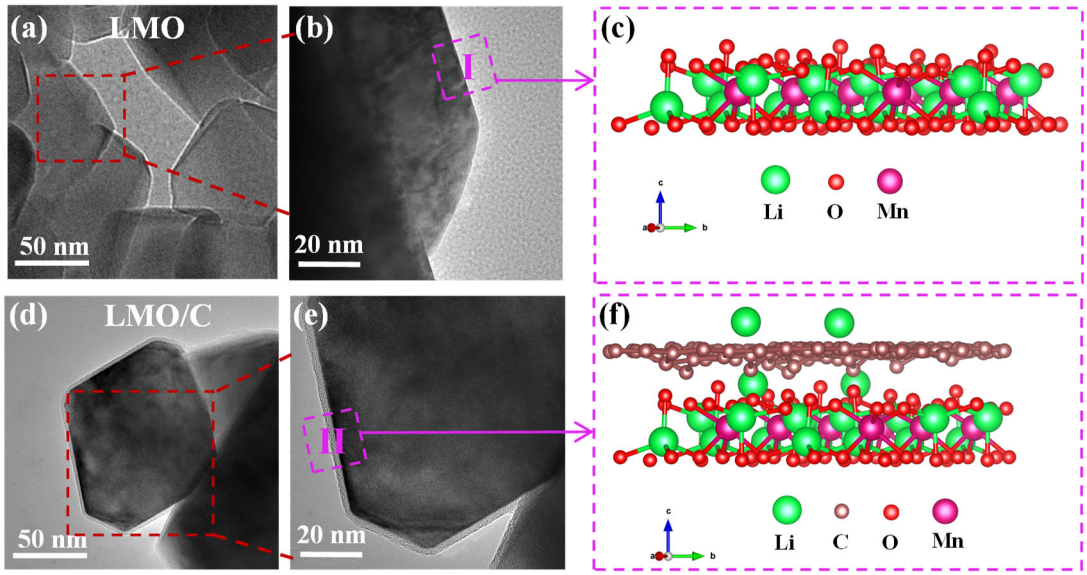

Fig. S9 Illustration of the charge storage mechanisms of the pristine LMO and LMO/C samples.

Fig. S10

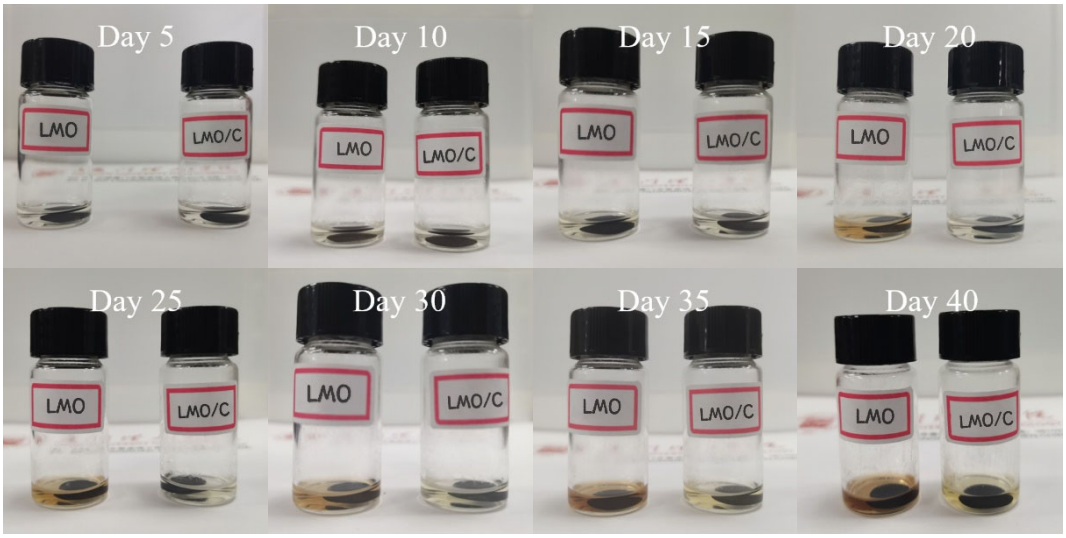

Fig. S10 Color changes of LMO/C and pristine LMO electrodes in 0.5 mL electrolyte.

Fig. S11

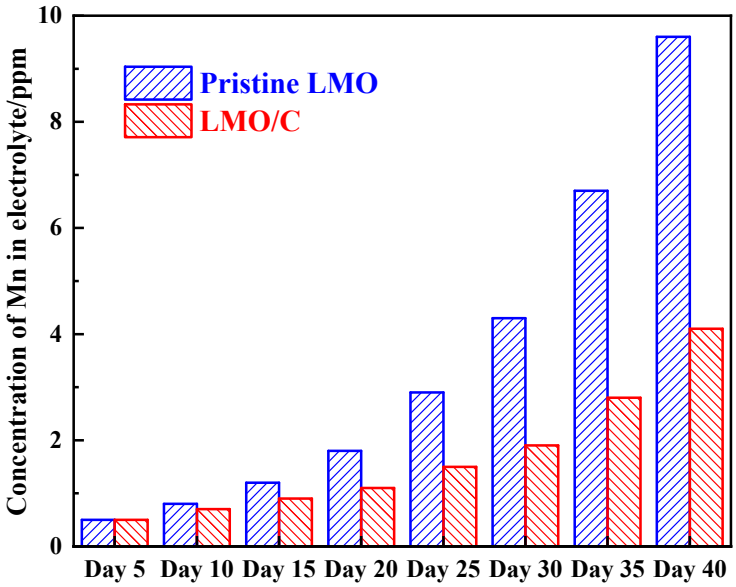

Fig. S11 Mn dissolution of LMO/C and pristine LMO electrodes in 0.5 mL electrolyte.

Fig. S12

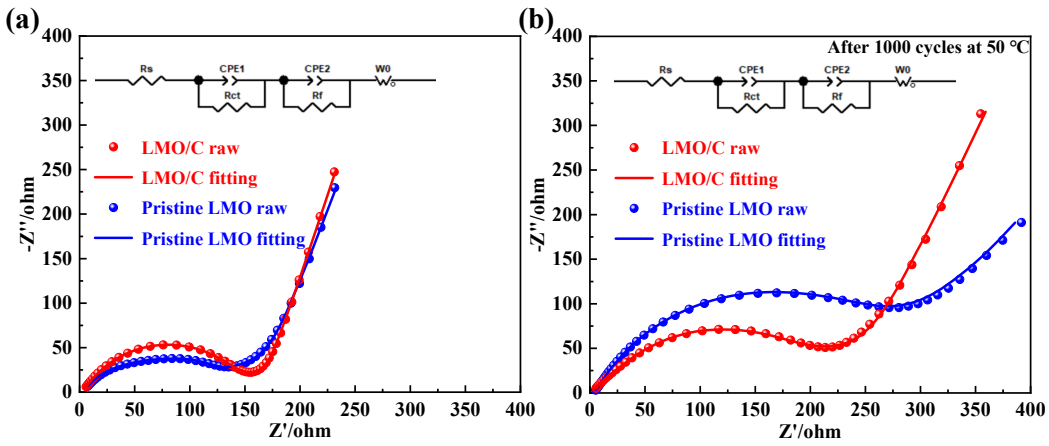

Fig. S12 The Nyquist plots of LMO/C and pristine LMO electrodes before cycling (a) and after 1000 cycles at 50 °C (c).

Table S1 The corresponding parameters of the LMO/C and pristine LMO electrodes before cycling and after 1000 cycles at 50 °C calculated from fitting the Nyquist plots with the equivalent circuit.

Sample	R_s (Ω)	CPE1-T (F)	CPE1-P	R_{ct} (Ω)	CPE2-T (F)	CPE2-P	R_f (Ω)	W_0-R	W_0-T	W_0-P
			Before cycling							
LMO	2.99	1.00×10^{-5}	0.73	60.54	1.53×10^{-5}	0.95	47.36	164.10	0.13	0.41
LMO/C	2.46	3.67×10^{-6}	0.85	75.20	4.85×10^{-5}	0.86	59.07	89.39	0.06	0.42
			After 1000 cycles at 50 °C							
LMO	3.46	1.35×10^{-5}	0.71	177.21	9.64×10^{-6}	0.88	82.30	120.50	0.18	0.37
LMO/C	1.80	1.05×10^{-5}	0.80	105.50	1.14×10^{-5}	0.81	63.46	218.50	0.12	0.39

Fig. S13

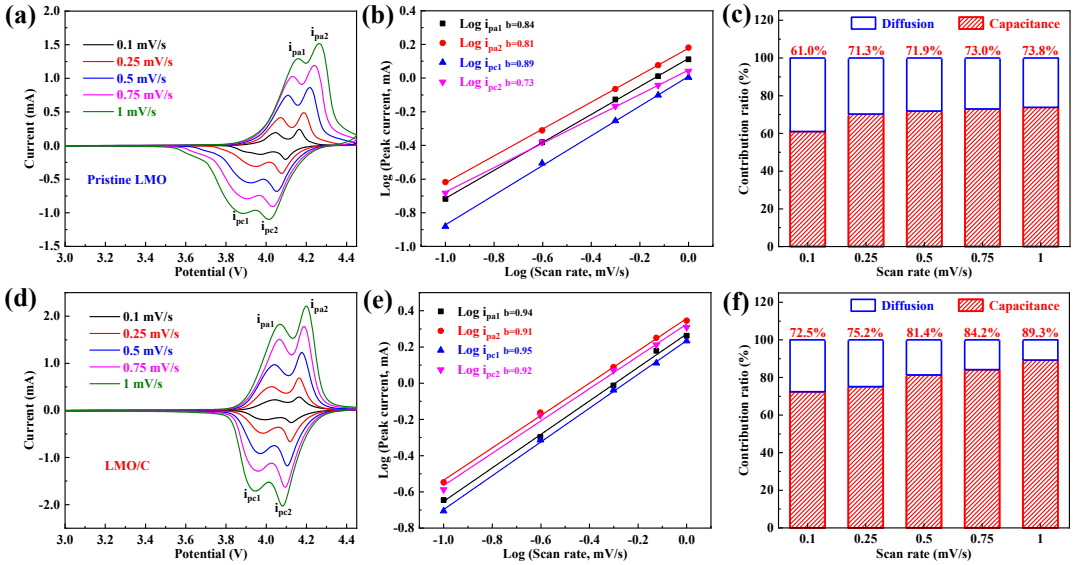

Fig. S13 CV curves at various scan rates from 0.1 to 1 mV/s (a, d), and their corresponding fitting b values of the two pairs of anodic/cathodic peaks (b, e), together with their pseudocapacitance-dominated contribution ratios at various scan rates (c, f) of the pristine LMO and the LMO/C electrodes respectively.

The peak current (i) and scan rate (υ) were log-fitted as a function of $\boldsymbol{i = a\upsilon^{b}}$ and the pseudocapacitance contribution ($k_1\upsilon$) and diffusion contribution ($k_2\upsilon^{1/2}$) can be calculated quantitatively by the formula $\boldsymbol{i\,(V) = k_1\upsilon + k_2\upsilon^{1/2}}$ [4].

Table S2 Comparison of cathode performance in coating $LiMn_2O_4$ between this work and previously reported.

Coating material	Testing temperature	Specific capacity	Cycle performance	Voltage range	Ref.
Al_2O_3	RT	120.4 mAh g^{-1} at 1 C	72.96% retained after 100 cycles	3.0-4.5 V	[5]
V_2O_5	55 °C	102.0 mAh g^{-1} at 0.2 C	92.30% retained after 100 cycles	3.0-4.3 V	[6]
Sm_2O_3	RT	101.6 mAh g^{-1} at 1 C	94.79% retained after 200 cycles	3.0-4.5 V	[7]
$MnBO_3$	RT	112.7 mAh g^{-1} at 1 C	85.20% retained after 1000 cycles	3.0-4.5 V	[8]
TiO_2	RT	85.0 mAh g^{-1} at 0.1 A g^{-1}	91.22% retained after 200 cycles	0.0-1.1 V	[9]
Li_2WO_4	55 °C	106.2 mAh g^{-1} at 1 C	90.54% retained after 100 cycles	3.0-4.3 V	[10]
Li_3PO_4	RT	124.3 mAh g^{-1} at 1 C	95.50% retained after 500 cycles	3.5-4.3 V	[11]
Carbon	RT	113.6 mAh g^{-1} at 1 C	92.00% retained after 1000 cycles	3.0-4.3 V	[12]
	RT	107.1 mAh g^{-1} at 1 C	79.00% retained after 1000 cycles	3.0-4.3 V	[13]
PVDF	RT	112.4 mAh g^{-1} at 0.1 C	80.00% retained after 500 cycles	3.0-4.3 V	[14]
Carbon	**50 °C**	**131.4 mAh g^{-1} at 5 C**	**92.92% retained after 1000 cycles**	**3.0-4.3 V**	**This work**

References

[1] L. Chen, Z. Xiong, Y. Cui, H. Luo, Y. Gao, *Appl. Surf. Sci.*, 2021, **542**, 148767.

[2] T. Li, Y. Gui, W. Zhao, C. Tang, X. Dong, *Phys. E Low-dimens. Syst. Nanostruct.*, 2020, **123**, 114178.

[3] T. Jiang, W. Zhang, T. Zhang, H. Yuan, M. Bi, X. Zhou, *Physica E*, 2023, **146**, 115568.

[4] J. Lin, Y. H. Sun, X. M. Lin, *Nano Energy*, 2022, **91**, 106655.

[5] H. Liu, F. Yang, J. Guo, M. Xiang, H. Bai, R. Wang, C. Su, *New J. Chem.*, 2021, **45**, 10534-10540.

[6] H. Ji, L. Ben, S. Wang, Z. Liu, R. Monteiro, R. Ribas, H. Yu, P. Gao, Y. Zhu, X. Huang, *ACS Appl. Energy Mater.*, 2021, **4**, 8350-8359.

[7] B. Zhang, Y. Zhang, B. Zhu, J. Duan, X. Li, X. Zeng, Z. Lian, R. Gong, K. Zhou, Z. Wang, Y. Gao, P. Dong, Y. Zhang, *Colloids Surf. A Physicochem. Eng. Asp.*, 2022, **646**, 128985.

[8] H. Li, L. Xue, M. Ni, S. V. Savilov, S. M. Aldoshin, H. Xia, *Electrochem. Commun.*, 2022, **137**, 107266.

[9] Y. Wu, M. Shi, D. Luo, Z. Zhang, Z. Li, Z. Cheng, X. Kang, *J. Electroanal. Chem.*, 2023, **943**, 117597.

[10] S. Wang, S. Jiang, Y. Li, Z. Tan, S. Hao, J. Yang, Z. He, *J. Power Sources*, 2023, **579**, 233292.

[11] J. Wang, Y. Xu, J. Wang, X. Ding, *J. Alloys Compd.*, 2023, **932**, 167642.

[12] X. Yu, J. Deng, X. Yang, J. Li, Z. H. Huang, B. Li, F. Kang, *Nano Energy*, 2020, **67**, 104256.

[13] C. Tomon, S. Sarawutanukul, N. Phattharasupakun, S. Duangdangchote, P. Chomkhuntod, N. Joraleechanchai, P. Bunyanidhi, M. Sawangphruk, *Commun. Chem.*, 2022, **5**, 54.

[14] C. L. Mu, M. Huang, H. L. Zhu, Y. X. Qi, Y. X. Wang, T. Li, Y. J. Bai, *Mater. Today Sustain.*, 2022, **18**, 100128.